



Review

Heterogeneous Cross-Coupling over Gold Nanoclusters

Quanquan Shi ^{1,2}, Zhaoxian Qin ² , Hui Xu ¹ and Gao Li ^{2,*}

¹ College of Science, Inner Mongolia Agricultural University, Hohhot 010018, China; qqshi@dicp.ac.cn (Q.S.); yqfxxuhui@163.com (H.X.)

² State Key Laboratory of Catalysis, Dalian Institute of Chemical Physics, Chinese Academy of Sciences, Dalian 116023, China; qinzhaoxian@dicp.ac.cn

* Correspondence: gaoli@dicp.ac.cn

Received: 23 April 2019; Accepted: 12 May 2019; Published: 1 June 2019



Abstract: Au clusters with the precise numbers of gold atoms, a novel nanogold material, have recently attracted increasing interest in the nanoscience because of very unique and unexpected properties. The unique interaction and electron transfer between gold clusters and reactants make the clusters promising catalysts during organic transformations. The Au_nL_m nanoclusters (where L represents organic ligands and *n* and *m* mean the number of gold atoms and ligands, respectively) have been well investigated and developed for selective oxidation, hydrogenation, photo-catalysis, and so on. These gold clusters possess unique frameworks, providing insights into the catalytic processes and an excellent arena to correlate the atomic frameworks with their intrinsic catalytic properties and to further investigate the tentative reaction mechanisms. This review comprehensively summarizes the very latest advances in the catalytic applications of the Au nanoclusters for the C–C cross-coupling reactions, e.g., Ullmann, Sonogashira, Suzuki cross-couplings, and A³–coupling reactions. It is found that the proposed catalytically active sites are associated with the exposure of gold atoms on the surface of the metal core when partial capping organic ligands are selectively detached under the reaction conditions. Finally, the tentative catalytic mechanisms over the ligand-capped Au nanoclusters and the relationship of structure and catalytic performances at the atomic level using computational methods are explored in detail.

Keywords: gold nanocluster; cross-coupling; Ullmann hetero-coupling; Sonogashira coupling; Suzuki coupling; A³–coupling; catalytic mechanism; ligand removal

1. Introduction

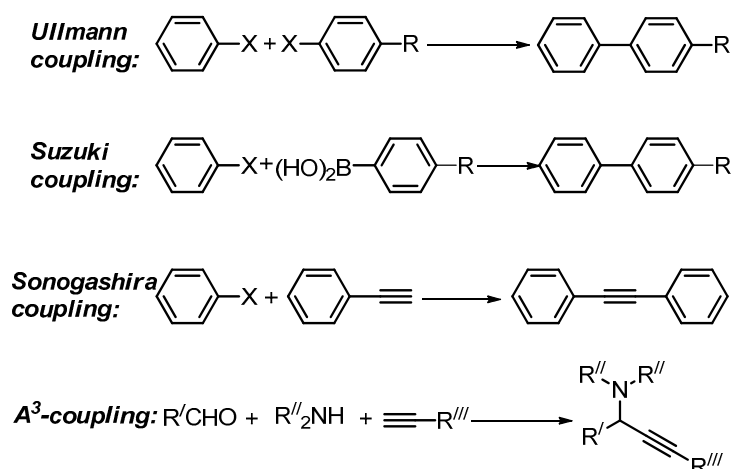
Since the work of Haruta's group in the late 1980s [1], supported gold nanoparticles with a particle size in the range of 3–20 nm have played a central role in a variety of reactions such as selective oxidation [2–5], hydrogenation [6–8], and photocatalysis [9,10]. These conventional gold catalysts have been realized via deposition–precipitation and co-precipitation impregnation with oxides by controlling the pH of the synthetic system. These obtained gold nanoparticles are usually polydisperse, which is a major issue in fundamental catalysis and investigations [11]. For example, the size-hierarchy of Au nanoparticles are often averaged out in polydispersion. It is difficult to correlate the relationship between the catalytic properties and the structure of the nanoparticles. Therefore, developing nanostructured catalysts with specific morphology (e.g., nanosheet, nanocube, and nanorod) is highly desirable to overcome this issue, further promoting the development of crystal-identified model catalysts [12,13].

On the other hand, the remarkable developments in the synthesis of atomically precise gold nanoclusters have been achieved in recent decades, which opens a new burgeoning area

in nanoscience [14,15]. These gold nanoclusters are comprised of a few dozen to a few hundred gold atoms and protecting organic ligands (e.g., thiolate, phosphine, and alkyne), and the size is ultra-small, usually ca. 0.6–2 nm. Some gold nanoclusters are identifiable by X-ray crystallography technology. It offers a big opportunity for in-depth understanding of the relationship of the catalytic properties and the active-site structure at the atomic level [16].

It is observed that these gold nanoclusters exhibit good catalytic performance in heterogeneous catalysis (e.g., selective oxidation and hydrogenation) [16–18]. Sometime, the gold clusters show better catalytic behavior (e.g., activity and product selectivity) than the corresponding Au nanoparticles, because of their high surface-to-volume ratio (reaches up to ~100%), surface geometric effect (e.g., low-coordinated $\text{Au}^{\delta+}$ atoms, $0 < \delta < 1$), and the unique electronic properties and the quantum size effect. Furthermore, the protecting organic ligands can improve the product selectivity due to their electronic factors and steric hindrance and weak interaction (e.g., π - π interaction) between the reactants and cluster surface ligands during the catalysis process. In the recent decade, these gold nanoclusters exhibited good catalytic activity in the cross C–C couplings, e.g., Ullmann hetero-coupling, Suzuki and Sonogashira coupling, and A^3 -coupling [19,20]. Traditionally, these catalyzed C–C coupling reactions are over the Cu, Pd, and Pt complexes and particles in the previous literatures [21–23].

In this review, we aim to provide an overview focused on the Au nanocluster-catalyzed coupling reactions, e.g., Ullmann hetero-coupling of Ar-I, Suzuki cross-coupling of PhB(OH)_2 and Ph-I (IB), Sonogashira cross-coupling of IB and $\text{Ph-C}\equiv\text{C-H}$ (PA), and A^3 -coupling (Scheme 1). The pathway of the selective detachment of the surface protecting ligands (under the reaction conditions), giving the catalytically active sites, is well discussed. Moreover, the proposed reaction pathway and mechanisms of these carbon–carbon coupling reactions were thoroughly summarized based on the precise framework of gold nanoclusters (e.g., two Au_{25}) as the mode theoretical calculations.



Scheme 1. Cross-coupling reactions over gold cluster in this review.

2. Activation of Ph-B(OH)_2 , Ph-I, and $\text{C}\equiv\text{C-H}$ Bonds over Au: Theoretical Simulation

The activation of the Ph-B(OH)_2 , Ph-I, and $\text{C}\equiv\text{C-H}$ bonds over the gold clusters plays an important role and step in the cross-coupling reactions, e.g., Ullmann hetero-coupling, Sonogashira coupling, Suzuki coupling, and A^3 -coupling. The adsorption and activation process of the reactants over the different well-defined gold facets and sites are distinct [24–27]. The density functional theory (DFT) calculations should be a feasible and fast method to explore the activation of Ph-B(OH)_2 , C-I, and $\text{C}\equiv\text{C-H}$ bond by gold nanoclusters.

Firstly, the shape controlled Au nanoparticles (e.g., Au nanorod) with well-defined surfaces and morphologies are well investigated [28,29], providing a platform to establish site–activity relationships and to pursue the understanding of heterogeneous processes. Therefore, the gold nanorod is chosen for the theoretical simulation of the activation of Ph-I and $\text{C}\equiv\text{C-H}$ bonds. DFT studies showed that

the Ph-I reactant adsorbs onto the Au(100) and Au(111) with Au-I distance 2.95 and 2.86 Å. The C-I bond is more elongated on the Au(111) compared to Au(100) (2.17 Å vs. 2.13 Å) [26]; the C-I length of the free IB is 2.09 Å. Furthermore, the phenyl group is located on an Au atom. The iodine atom is strongly chemisorbed on the bridging and hollow sites. Regarding the activation of alkyne, the Ph-C≡C- fragment is also adsorbed on bridging and 3-fold hollow sites of Au(100) and Au(111). The coordination number of one Ph-C≡C- unit is 3 and 4 for Au(100) and Au(111) facets during the cross-coupling reaction, respectively, Figure 1, and the activation energy of cross-coupling is comparable [26].

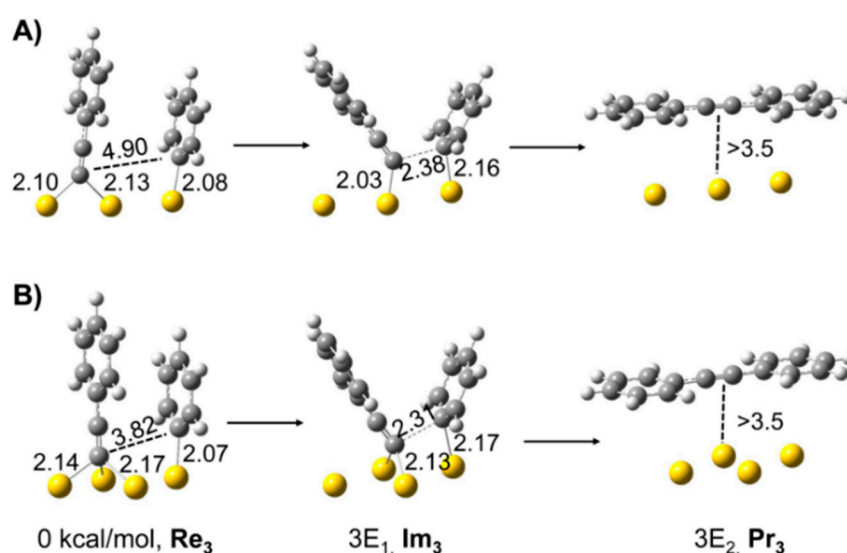


Figure 1. Proposed pathway for the cross-coupling on the (A) Au(100) and (B) Au(111). Reproduced with permission from [26]. Elsevier, 2015.

Next, the activation of Ph-B(OH)₂, Ph-I, and C≡C-H also was explored on a model cluster (Au₃₈ and partially oxidized Au₃₈O₂) [30–32]. It is worthy to note that the model clusters of the Au₃₈ and Au₃₈O₂ are somewhat different from the real catalyst in terms of the real structure. The Au₃₈O₂ cluster contains metallic Au⁰ and cationic Au^{δ+} species, and each O atom bonds to three Au atoms. In the activation process of phenylboronate, DFT showed that the phenylboronate reactant is preferentially adsorbed on the Au⁰ species rather than on the Au^{δ+} sites [30], leading to formation of the final product- biphenyl (Figure 2B). Meanwhile, DFT simulation also found that the interaction between the Au^{δ+} sites and Ph-I is weaker and the adsorption of C≡C-H on Au^{δ+} sites is relatively strong. Further, the proton of alkyne was detached with aid of O atom in the deprotonation step (Figure 2A). Therefore, a very low activation energy is required when the cross-coupling reactions occurred over the Au₃₈O₂ cluster. Of note, the cross-coupling step of the activated PA and -Ph on the Au₃₈O₂ should be the rate-determining step [32].

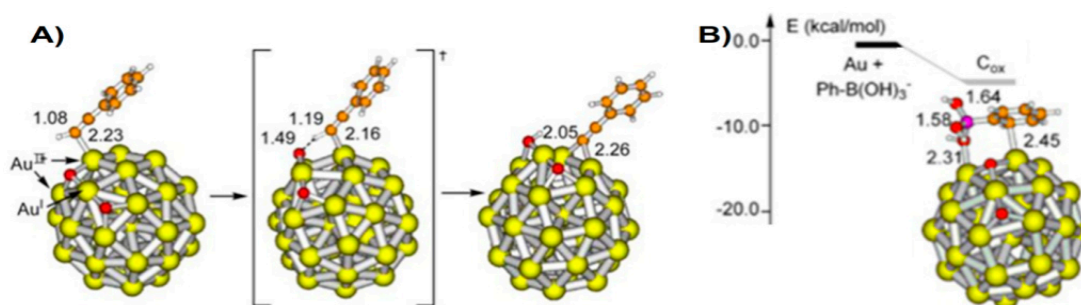


Figure 2. Calculated energy of the dissociation of PhB(OH)₃⁻ anion (A) and deprotonation of PA (B) on the Au₃₈O₂ cluster. Reproduced with permission from [30]. American Chemical Society, 2012.

3. Physical Property of Au Nanoclusters

3.1. Framework

The gold clusters with crystal structure can be employed as the practical simulation models for mechanism study. In this Review, we only focus on the two cluster structures of the nanorod-shaped $[\text{Au}_{25}(\text{PPh}_3)_{10}\text{L}_5\text{Cl}_2]^{2+}$ ($\text{L} = -\text{SR}$ and PA) and the nanosphere $[\text{Au}_{25}(\text{SR})_{18}]^x$ ($x = -1, 0, +1$, etc.), used as the real model for DFT studies (*vide infra*). The $\text{Au}_{25}(\text{SR})_{18}$ cluster comprises an Au_{13} core [33] and six staples of $\text{Au}_2(\text{SR})_3$ [34]. $[\text{Au}_{25}(\text{PPh}_3)_{10}\text{L}_5\text{Cl}_2]^{2+}$ is composed of two Au_{13} cores by sharing one common vertex to form the waist sites [35], connected by thiolate or alkyne ligands [36] (Figure 3).

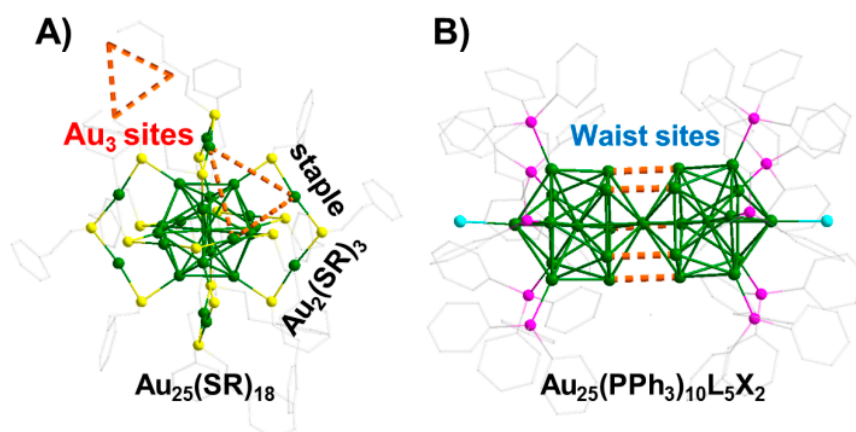


Figure 3. Framework of $\text{Au}_{25}(\text{SR})_{18}$ (A) and $\text{Au}_{25}(\text{PPh}_3)_{10}\text{L}_5\text{Cl}_2$ (B). The orange areas in are the Au_3 and the waist active sites during the catalysis. Reproduced with permission from [36]. American Chemical Society, 2008 and Springer, 2019.

3.2. Redox Property of Au cluster

$\text{Au}_{38}\text{S}_2(\text{SAdm})_{20}$ ($\text{SAdm} = \text{adamantanethiolate}$) nanoclusters exerted photosensitizing properties to give singlet oxygen ($^1\text{O}_2$) under visible light irradiation (e.g., 532 and 650 nm) [37]. The $\text{Au}_{38}\text{S}_2(\text{SAdm})_{20}$ is intact during the whole photocatalysis process, evidenced by UV-vis tracing and mass spectroscopy analysis. The cyclic voltammetry analysis showed that the $\text{Au}_{38}\text{S}_2(\text{SAdm})_{20}$ cluster had good charge transfer capacity to the redox $\text{K}_3\text{Fe}(\text{CN})_6$ probe, Figure 4 [38]. However, the redox property of the cluster disappeared when β -cyclodextrins (β -CDs) was introduced in the THF solution. After detailed analysis, the huge β -CDs “umbrella” can trap the adamantane groups and then completely cover windows of the $\text{Au}_{38}\text{S}_2(\text{SAdm})_{20}$ nanoclusters, thereby blocking direct interaction with foreign molecules and then quenching the charge transfer process (Figure 4B). It indicated that these gold nanoclusters have good redox properties and electron transfer (ET) capacity during the catalytic reactions [39].

Further, Kumar and coworkers studied the $\text{Au}_{25}(\text{SG})_{18}$ catalyst in an electrochemical oxidation [40]. The $\text{Au}_{25}(\text{SG})_{18}$ on the electrode gave good electro-activity during the oxidation of ascorbic acid and dopamine over a wide linear range from 0.71 to 44.4 μM . And pH dependent electrocatalytic activity was observed, attributed to the consequence of pH-dependent electrostatic attraction/repulsion between the charged $\text{Au}_{25}(\text{SG})_{18}$ clusters and the charged analytes. Moreover, an amperometric sensing method for other compounds was developed. Next, Kauffman et al. investigated the electron transfer between CO_2 and $\text{Au}_{25}(\text{PET})_{18}$ in solution [41]. Upon the DMF solution (containing $\text{Au}_{25}(\text{SR})_{18}$) was saturated with CO_2 gas, the optical absorbance features showed the oxidized state of $\text{Au}_{25}(\text{SR})_{18}$. Meanwhile, the photoluminescence increases and blue-shift. The CO_2^- induced optical changes can be simply reversed by purging the solution with N_2 gas to remove the CO_2 , indicating an interaction between $\text{Au}_{25}(\text{SR})_{18}$ and CO_2 . DFT calculations revealed that the CO_2 molecule interacts with three S atoms of the Au_3 site of the $\text{Au}_{25}(\text{SR})_{18}$ cluster, prompting the CO_2 electrochemical reduction. These observed unique

interactions and electron transfers between gold clusters and reactants make the clusters promising catalysts during the organic transformations.

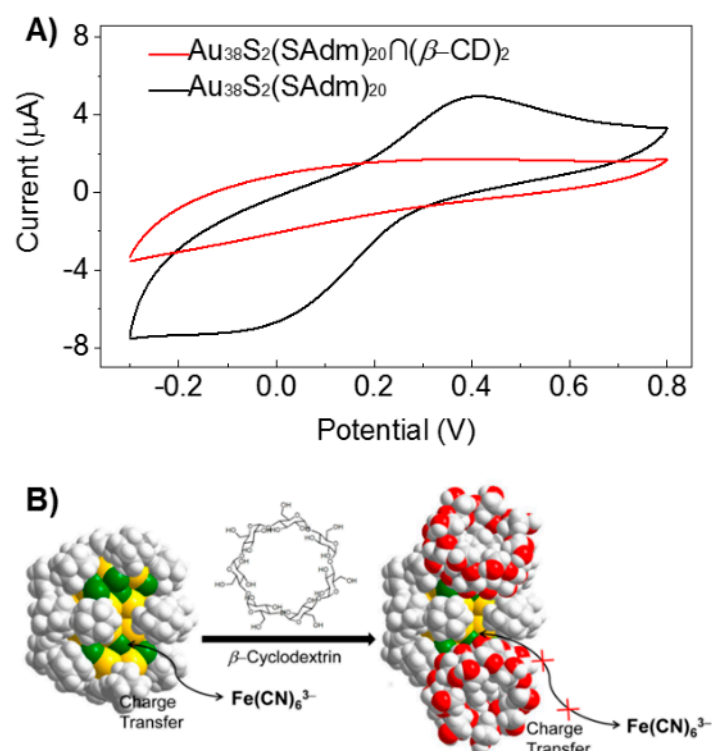


Figure 4. (A) Cyclic voltammograms (CV) for the redox reaction in potassium ferricyanide solution on $\text{Au}_{38}\text{S}_2(\text{SAdm})_{20}$ clusters and $\text{Au}_{38}\text{S}_2(\text{SAdm})_{20}-(\beta\text{-CD})_2$ conjugates. (B) Schematic illustrations of the $\text{Au}_{38}\text{S}_2(\text{SAdm})_{20}-(\beta\text{-CD})_2$ formation and the charge transfer between $\text{Fe}(\text{CN})_6^{3-}$ and the Au clusters and conjugates. Reproduced with permission from [38]. The Royal Society of Chemistry, 2016.

4. Catalytic Properties

4.1. Ullmann Coupling

At the beginning, the catalytic activity of the Au nanoclusters was examined in the Ullmann homo-coupling reactions of aryl iodides, which are generally catalyzed by palladium, nickel, and copper catalysts [42]. The supported gold cluster catalysts were simply prepared by a vortex-mixing of supports and a solution containing gold clusters at room temperature, and an annealing at 150 °C. The supported Au clusters were intact after the 150 °C annealing process (higher than the reaction temperatures), evidenced by UV–vis and scanning transmission electron microscopy (STEM) [43]. The X-ray photoelectron spectroscopy (XPS) analysis shows the chemical state of Au species in the oxide-supported cluster catalysts is positively charged ($\text{Au}^{\delta+}$) [44], where $0 < \delta < 1$, consistent with the free gold nanoclusters. The catalytic processes were carried out at 130 °C in the presence of base, which is similar with these catalyzed by Pd/Cu complexes or nanoparticles. The $\text{Au}_{25}(\text{SR})_{18}/\text{CeO}_2$ showed the best catalytic activity, and the test was then expanded to a serial of substituents with functional side-groups (Table 1) [45]. Of note, the efficiency of gold nanoclusters was not as good as the palladium, nickel, and copper nanocomposites in the Ullmann homo-coupling reactions of aryl chlorides and aryl bromides.

Table 1. The catalytic results over the Au₂₅(PET)₁₈/CeO₂ catalysts in Ullmann homo-coupling. Reaction conditions: 0.2 mmol iodobenzene, 0.6 mmol K₂CO₃, 100 mg Au₂₅(PET)₁₈/CeO₂ (1 wt% cluster loading), 1 mL DMF, 130 °C, 2 day.

Entry	Substrate	Product	Conversion (%)
1			99.8
2			99.5
3			67.5
4			78.2
5			99.7

Later, these Au cluster were studied in the Ullmann hetero-coupling reactions. The catalytic conditions over the Au₂₅(SR)₁₈/CeO₂ catalysts were the same with the homo-coupling reactions (Table 1 vs. Table 2). The aromatic and aliphatic thiolate-capped Au₂₅ nanoclusters (e.g., naphthalenethiolate (-SNap), benzenethiolate (-SPh), hexanethiolate (-SC₆H₁₃), and 2-phenylethanethiolate (PET)) were chosen for comparison and exploration in the Ullmann hetero-coupling of 4-MeC₆H₄I and 4-NO₂C₆H₄I [46]. Intriguingly, the aromatic thiolate ligated Au₂₅ clusters gave much better catalytic performance (both the conversion of NO₂C₆H₄I and selectivity for the hetero-coupling product (4-methyl-4'-nitrobiphenyl) than these protected by alkyl thiolate ligands. The Au₂₅(SNap)₁₈ cluster gave an 82% selectivity toward the hetero-coupling product, which was much higher than the Cu, Pd, and Au complexes (the selectivity: <30%, Table 2). Unfortunately, both of the conversion and selectivity decreased in the 2nd and 3rd cycles, which was due to the removal of the capping surface ligands and hence the decomposition of Au clusters, evidenced by the TEM images. These large gold nanoparticles jeopardized the catalytic performance in this coupling reaction. Thus, the protecting ligands on the clusters' surface play a key influence on their catalytic properties.

Table 2. The catalytic results over the Au₂₅(SR)₁₈/CeO₂ catalysts in Ullmann hetero-coupling. Reaction conditions: 0.06 mmol 4-methyl iodobenzene, 0.05 mmol 4-nitroiodobenzene, 0.3 mmol K₂CO₃, 100 mg Au₂₅(SR)₁₈/CeO₂ (~1 wt % cluster loading), 1 mL DMF, 130 °C, 24 h.

Catalyst	Conversion (%)	Selectivity (%)
Au ₂₅ (SC ₆ H ₁₃) ₁₈	69	16
Au ₂₅ (PET) ₁₈	72	19
Au ₂₅ (SPh) ₁₈	80	50
Au ₂₅ (SNap) ₁₈	91	82

DFT simulations were applied to explain the catalytic results. It is worthy to note that the reactants of both 4-MeC₆H₄I and 4-NO₂C₆H₄I cannot interact well with the intact Au₂₅(SR)₁₈ clusters, because of the steric effect of the protecting thiolate ligands on the clusters' surface. In the first step, one “-SR” unit on the Au₂₅(SR)₁₈ cluster was surmised to be detached under the reaction conditions in the presence of a K₂CO₃ base. Then the gold atoms on the motif were exposed to reactants and were associated with the catalytic sites [44]. Further, the activation energy for the homo- and hetero-couplings over the Au₂₅ protected by “-SCH₃” thiolate were compared by the nudged elastic band (NEB) approach (Figure 5). Intriguingly, the activation energy in the hetero-coupling was less than in the homo-coupling in the case of Au₂₅-S Nap clusters, (Figure 4). It implied that the aromatic thiolate-capped gold cluster can not only improve the conversion rate but can also favor the hetero-coupled process [46].

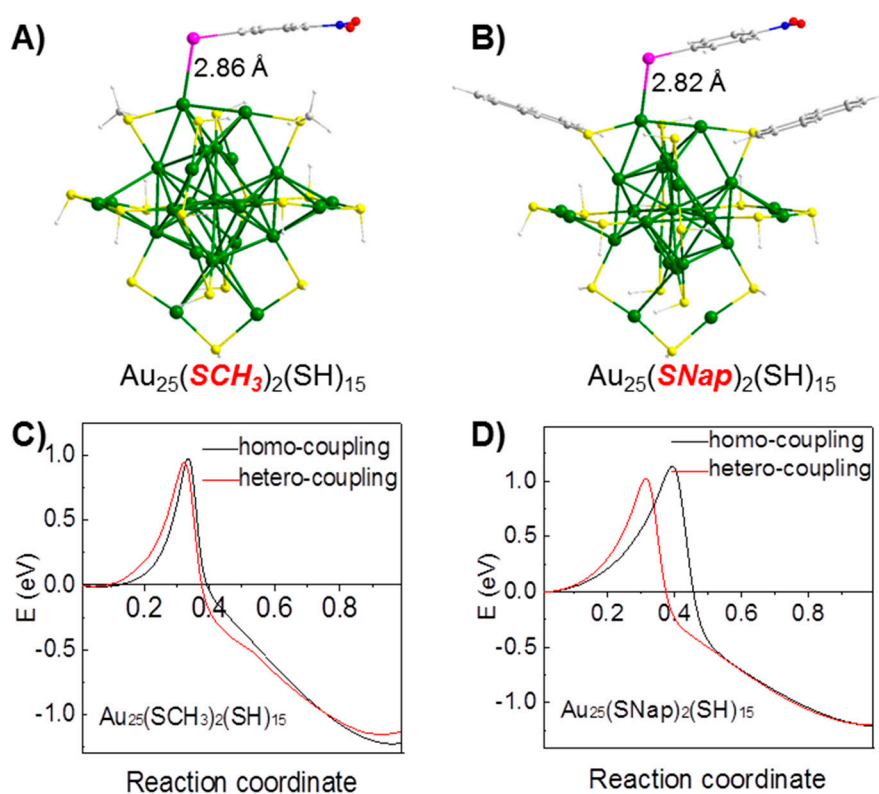


Figure 5. Interaction of 4-NO₂C₆H₄I with the exposed Au atoms on the Au₂₅(SCH₃)₂(SH)₁₅ (A) and Au₂₅(SNap)₂(SH)₁₅ (B). Energy vs. reaction coordinate with “-SCH₃” (C) and “-SNap” ligands (D) during the homo- and hetero-coupling reactions. Reproduced with permission from [46]. American Chemical Society, 2016.

DFT simulations were applied to explain the catalytic results. It is worthy to note that the reactants of both 4-MeC₆H₄I and 4-NO₂C₆H₄I cannot interact well with the intact Au₂₅(SR)₁₈ clusters, because of the steric effect of the protecting thiolate ligands on the clusters' surface. In the first step, one “-SR” unit on the Au₂₅(SR)₁₈ cluster was surmised to be detached under the reaction conditions in the presence of K₂CO₃ base. Then the gold atoms on the motif were exposed to reactants and were associated with the catalytic sites [44]. Further, the activation energy for the homo- and hetero-couplings over the Au₂₅ protected by “-SCH₃” thiolate are comparable by the nudged elastic band (NEB) approach (Figure 5). Intriguingly, the activation energy in the hetero-coupling less than in the homo-coupling in the case of Au₂₅-S Nap clusters, (Figure 4). It implied that the aromatic thiolate-capped gold cluster not only can improve the conversion rate but also can favor the hetero-coupled process [46].

4.2. Suzuki Coupling

Further, the titania-supported Au₂₅ clusters are studied in the Suzuki coupling in the presence of ionic liquids (ILs), which are catalyzed over palladium catalysts [42]. The Suzuki cross-coupling run at 90 °C using different solvents (e.g., ethanol, xylene, toluene, *N,N'*-dimethylformamide (DMF), ILs, etc.). The imidazolium-based ILs exerted a large effect on the MeOC₆H₄I conversion to the desire products. A very low conversion (<5%) is observed when using the ethanol, toluene, *o*-xylene, and DMF as solvents in the Au₂₅/TiO₂ catalyzed coupling reactions (Table 3). Interestingly, the iodoanisole conversion over Au₂₅/TiO₂ drastically increased to 89%–99% when BMIM·X (BMIM: 1-butyl-3-methylimidazolium, X = Br or Cl or BF₄) solvents are introduced to the reaction system (Table 3). The catalytic results indicate that the imidazolium-based ILs acts as a promoter for the cross-coupling reactions [47]. Of note, only the BMIM cation (i.e., the acidic proton at position 2 of the imidazolium ions) play an important role during the reactions, as no activity is found in the presence of BDiMIM·BF₄ (BDiMIM: 1-butyl-2,3-dimethylimidazolium) solvent, which is further supported by the DFT calculations. It is worthy to note that the efficiency of gold nanoclusters was not as good as the palladium nanocomposites, however, the gold nanoclusters exhibited much better selectivity toward the target cross-coupling products.

Table 3. Catalytic results over the Au₂₅/TiO₂ catalysts in the Suzuki cross-coupling reactions of iodoanisole and phenylboronic acid using the imidazolium-based ionic liquids. Reaction conditions: 0.1 mmol iodoanisole, 0.12 mmol phenylboronic acid, 0.36 mmol K₂CO₃, 100 mg Au₂₅(SR)₁₈/TiO₂ (~1 wt % cluster loading), solvents (1 mL EtOH or EtOH:H₂O (10:1, *v/v*), and 0.2 mL IL or other organic solvents), 90 °C, 18 h.

Solvent	Conversion (%)
o-xylene + EtOH:H ₂ O	<0.5
DMF + EtOH:H ₂ O	4
BMIM·Br + EtOH	89
BMIM·Cl + EtOH	90
BMIM·BF ₄ + EtOH	94
BMIM·BF ₄ + EtOH:H ₂ O	>99
BDiMIM·BF ₄ + EtOH	<0.5

To explore the active species during the coupling reactions, the free Au₂₅(PET)₁₈ was mixed with the BMIM·BF₄ under the same reaction conditions [43]. Except the molecular peak of Au₂₅(PET)₁₈ cluster, four new mass peaks are clearly detected in the matrix-assisted laser desorption/ionization mass spectrometry (MALDI-MS). These new appeared mass peaks belonged to the Au_{25-n}(SR)_{18-n} (where, *n* = 1–4) species (Figure 6). Of note, these new species are not the fragments caused by laser of the MALDI method. These species also were observed in the ESI-MS method [48]. The imidazolium-based ILs indeed assist the yield of Au_{25-n}(SR)_{18-n} species under the reaction conditions, which may be the active sites for the cross-coupling reactions. The other explanation is that the Au-NHC complex (NHC: N-heterocyclic carbene) with the Au_{25-n}(SR)_{18-n} species could be responsible for the active sites during the Suzuki cross-coupling reactions, although it needs further investigation. Of note, the Au-NHC complex was the product of the reaction of BMIM cations with the gold nanoclusters.

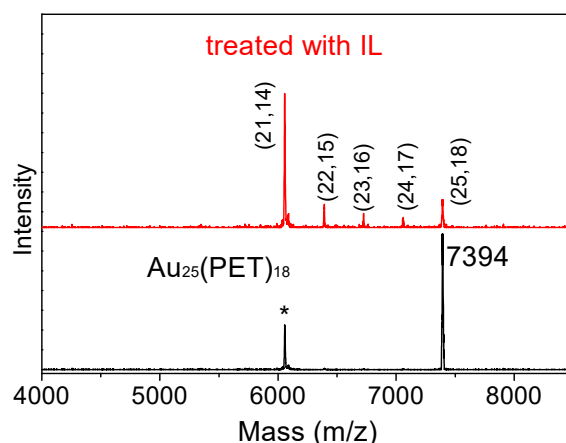


Figure 6. Matrix-assisted laser desorption/ionization mass spectrometry (MALDI-MS) of the fresh $\text{Au}_{25}(\text{PET})_{18}$ clusters and samples treated with the ionic liquid (IL) of BMIM- BF_4 ; the (n, m) presents the number of the $\text{Au}_n(\text{PET})_m$ species. Reproduced with permission from [47]. American Chemical Society, 2015.

4.3. Sonogashira Coupling

As the IB and alkyne can be activated over gold clusters, hence, the catalytic performance of the gold nanoclusters may extend to Sonogashira cross-coupling reactions, often catalyzed over palladium catalysts [42]. The catalytic performance of the $\text{Au}_{25}(\text{PET})_{18}$ cluster (supported on oxides) in the Sonogashira cross-coupling reaction was studied [49]. The supported catalyst was prepared by impregnating oxide powders (such as TiO_2 , CeO_2 , SiO_2 , and MgO) in a CH_2Cl_2 solution of $\text{Au}_{25}(\text{PET})_{18}$ (~1 wt % loading) with a 150 °C annealing. STEM and TG analyses showed that the protecting thiolate ligands were intact on the surface of gold clusters after thermal treatment. Then these Au_{25} /oxide catalysts were applied to the Sonogashira cross-coupling reaction. The optimized reaction conditions were using DMF as a solvent and K_2CO_3 as a base under an N_2 atmosphere at 160 °C, which is harsher than those for the above Suzuki and Ullmann couplings. The $\text{Au}_{25}/\text{CeO}_2$ catalyst showed the best activity (96.1% iodoanisole conversion with 88.1% selectivity toward the target product) (Table 4). The solvent and base can also influence the product selectivity. The size-dependent catalytic performance also was studied.

Table 4. The catalytic performance of $\text{Au}_{25}(\text{SR})_{18}$ /oxides in the Sonogashira cross-coupling reaction of p-iodoanisole and phenylacetylene. DMBP and MPEB stand for homo-coupling product of 4,4'-dimethoxy-1,1'-biphenyl and cross-coupling product of 1-methoxy-4-(2-phenylethynyl)benzene, respectively. Reaction conditions: 100 mg catalyst (1 wt % $\text{Au}_{25}(\text{SR})_{18}$ or AuNC 2–3 nm (SC_6H_{13}) loading), 0.1 mmol p-iodoanisole, 0.15 mmol phenylacetylene, 0.3 mmol K_2CO_3 , 1 mL DMF, 160 °C, 40 h. n.r. = no reaction. Conv. = conversion.

Entry	Catalyst	Conv. (%)	Selectivity (%)	
			MPEB	DMBP
1	$\text{Au}_{25}(\text{SR})_{18}/\text{CeO}_2$	96.1	88.1	11.9
2	$\text{Au}_{25}(\text{SR})_{18}/\text{TiO}_2$	92.8	82.9	17.1
3	$\text{Au}_{25}(\text{SR})_{18}/\text{SiO}_2$	90.8	79.3	20.7
4	$\text{Au}_{25}(\text{SR})_{18}/\text{MgO}$	93.3	80.6	19.4
5	AuNC 2–3 nm (SC_6H_{13})/ CeO_2	65.5	57.2	42.8
6	CeO_2	n.r.		
7	TiO_2	n.r.		

The catalytic performance of small-sized $\text{Au}_{25}(\text{PET})_{18}$ cluster catalysts was much better than large-sized of gold clusters of 2–3 nm and Au/ CeO_2 (~20 nm). Support effects were studied in the

cross-coupling, and no distinct effect of the oxide supports was observed (i.e., CeO₂, SiO₂, TiO₂, and MgO). The conversion was no obvious decrease, but the selectivity decreased from 88.1% to 64.5% after 5 cycles. It is noteworthy that TEM analysis shows that the gold clusters grow into larger nanoparticles (>3 nm), meaning that the gold clusters capped by organic ligands cannot stay intact under harsh reaction conditions (160 °C in the presence of a base). The gradual degradation of gold clusters leads to a decrease in selectivity, as the larger Au clusters showed a much lower selectivity. It is worthy to note that the efficiency of gold nanoclusters is much worse than the palladium-based catalysts, and the selectivity for the cross-coupling products over Au clusters is also worse.

DFT calculation found that the reactants (i.e., IB and PA) prefer to adsorb on the open facet (Au₃) of the Au₂₅ cluster with the phenyl ring facing a surface Au atom (Figure 7). A total adsorption energy reaches −0.90 eV when the two reactants co-adsorb on the Au₂₅(SR)₁₈ catalyst. While, the IB/IB pair has an adsorption energy of −1.05 eV, indicating that the IB/IB pair interacts strongly with the cluster and the homocoupling of IBs is the dominant side-reaction competing with the cross-coupling between IB and PA. DFT results suggested that the catalytic active sites is associated with the Au₂₅(SR)₁₈ clusters, which is consistent with the experimental results.

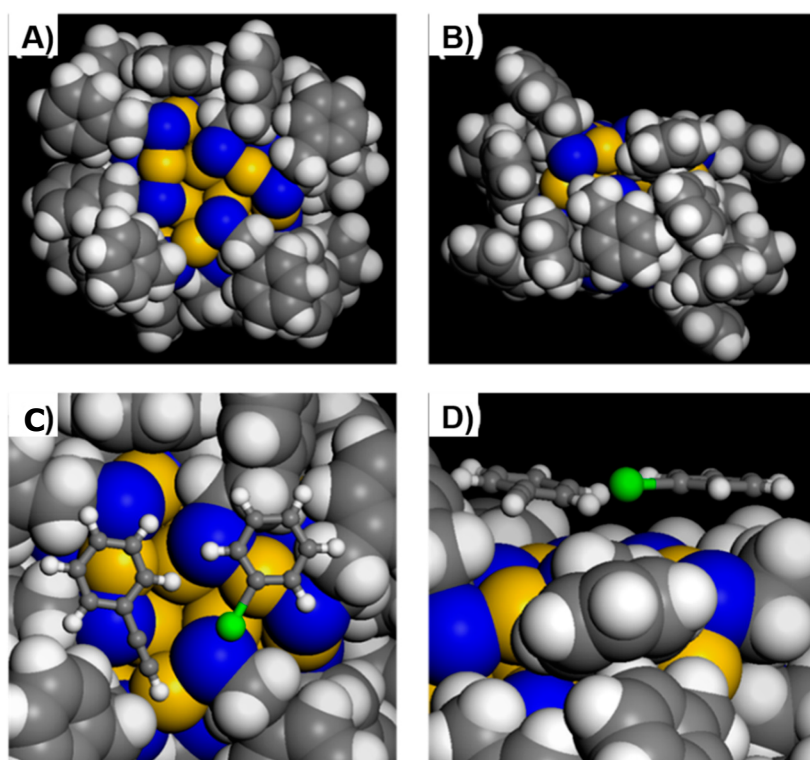
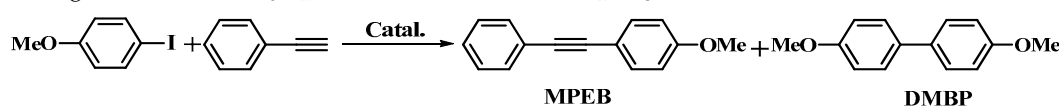


Figure 7. (A) Top view of one of the two open facets of Au₂₅(PET)₁₈ clusters where three external Au atoms are exposed; the other facet is on the back side. (B) Side view of the two facets which are at top and bottom. (C) Top view and (D) side view of the co-adsorption of PA and IB on the surface of the Au₂₅(PET)₁₈ clusters. Color code: Au, yellow; S, blue; C, gray; H, white; I, green. Reproduced with permission from [49]. Elsevier, 2013.

The structure of the 25-atom cluster is similar [50], but the electronic property and the catalytic activity of the bimetallic clusters can be largely regulated by the foreign dopants [50–55]. Recently, Li et al. [56] studied the doping effects of the Au₂₅(SR)₁₈ nanoclusters in the Sonogashira cross-coupling reaction base on the experiment and DFT simulations. The obtained results suggested that the Cu and Ag atoms are preferentially occupied at the cluster's kernel (Au₁₃) rather than the Au₂(SR)₃ staple motif, while a single Pt atom only can be doped individually and locates in the center of the cluster. The overall performance of Ag_xAu_{25-x}(SR)₁₈ was similar to that of Au₂₅(SR)₁₈ and Pt₁Au₂₄(SR)₁₈,

which showed a decrease in catalytic activity (Table 5). The catalytic activity was from $\text{Ag}_x\text{Au}_{25-x}(\text{SR})_{18} \approx \text{Au}_{25}(\text{SR})_{18} > \text{Cu}_x\text{Au}_{25-x}(\text{SR})_{18} > \text{Pt}_1\text{Au}_{24}(\text{SR})_{18}$. Interestingly, the $\text{Cu}_x\text{Au}_{25-x}(\text{SR})_{18}$ produced a homo-coupling product base on the Ullmann homo-coupling pathway, which is contrary to the other three cluster catalysts. However, DFT calculations showed that the adsorption energy of one PA molecule on the $\text{Pt}_1\text{Au}_{24}(\text{SR})_{18}$, $\text{Cu}_{1/2}\text{Au}_{24/23}(\text{SR})_{18}$, and $\text{Au}_{25}(\text{SR})_{18}$ nanoclusters was very similar (-0.50 to -0.52 eV, Table 6). The adsorption energy of one IB molecule onto the $\text{Pt}_1\text{Au}_{24}(\text{SR})_{18}$, $\text{Ag}_{1/2}\text{Au}_{24/23}(\text{SR})_{18}$ and $\text{Au}_{25}(\text{SR})_{18}$ was also very similar (-0.59 to -0.61 eV, Table 6). These results suggested that the adsorption process of the PA and IB onto the alloy clusters is not the key step during the coupling reactions. Generally, the catalytic activity is largely affected by the electronic effect in the core of bimetallic clusters (i.e., $\text{Pt}_1\text{Au}_{12}$, $\text{Cu}_x\text{Au}_{13-x}$, $\text{Ag}_x\text{Au}_{13-x}$, and Au_{13}), and the selectivity of product is primarily turned by the atomic type on the shell of $\text{M}_x\text{Au}_{12-x}$ [51,57].

Table 5. Catalytic performance of TiO_2 -supported $\text{M}_x\text{Au}_{25-x}(\text{SR})_{18}$ catalysts in the C–C coupling reaction between $\text{MeOC}_6\text{H}_4\text{I}$ and PA. Reaction conditions: 100 mg catalyst, 1 wt % $\text{M}_x\text{Au}_{25-x}(\text{SR})_{18}$ loading, 0.1 mmol $\text{MeOC}_6\text{H}_4\text{I}$, 0.1 mmol PA, 0.3 mmol K_2CO_3 , 1 mL DMF, 160 °C, 40 hr.



Entry	Catalysts	Conversion (%)	Selectivity (%)	
			MPEB	DMBP
1	$\text{Au}_{25}(\text{SR})_{18}$	79.5	65.7	34.3
2	$\text{Ag}_x\text{Au}_{25-x}(\text{SR})_{18}$	83.0	55.4	44.6
3	$\text{Cu}_x\text{Au}_{25-x}(\text{SR})_{18}$	52.4	28.3	71.7
4	$\text{Pt}_1\text{Au}_{24}(\text{SR})_{18}$	48.5	67.2	32.9

Table 6. Adsorption energy of the PA and IB on the Au_3 site of the $\text{M}_1\text{Au}_{24}(\text{SR})_{18}$ (M: Pt, Ag, and Cu, and noted as M_1Au_{24}) and $\text{M}_2\text{Au}_{23}(\text{SR})_{18}$ (M: Ag and Cu, M_2Au_{23}) cluster models, respectively.

Adsorption Energy (eV)	$\text{M}_x\text{Au}_{25-x}(\text{SR})_{18}$ Cluster					
	Au_{25}	$\text{Pt}_1\text{Au}_{24}$	$\text{Ag}_1\text{Au}_{24}$	$\text{Ag}_2\text{Au}_{23}$	$\text{Cu}_1\text{Au}_{24}$	$\text{Cu}_2\text{Au}_{23}$
One PA	-0.51	-0.50	-0.61	-0.60	-0.52	-0.52
One IB	-0.60	-0.61	-0.59	-0.59	-0.54	-0.58
“PA + IB” pair	-1.11	-1.11	-1.20	-1.19	-1.06	-1.10
“IB + IB” pair	-1.20	-1.22	-1.18	-1.18	-1.08	-1.16

The structure of the 25-atom cluster was similar [50], but the electronic property and the catalytic activity of the bimetallic clusters could be largely regulated by the foreign dopants [50–55]. Recently, Li et al. [56] studied the doping effects of the $\text{Au}_{25}(\text{SR})_{18}$ nanoclusters in a Sonogashira cross-coupling reaction based on an experiment and DFT simulations. The obtained results suggested that the Cu and Ag atoms were preferentially occupied at the cluster’s kernel (Au_{13}) rather than the $\text{Au}_2(\text{SR})_3$ staple motif, while a single Pt atom only can be doped individually and locates in the center of the cluster. The overall performance of $\text{Ag}_x\text{Au}_{25-x}(\text{SR})_{18}$ was similar to that of $\text{Au}_{25}(\text{SR})_{18}$ and $\text{Pt}_1\text{Au}_{24}(\text{SR})_{18}$, which showed a decrease in catalytic activity (Table 5). The catalytic activity was $\text{Ag}_x\text{Au}_{25-x}(\text{SR})_{18} \approx \text{Au}_{25}(\text{SR})_{18} > \text{Cu}_x\text{Au}_{25-x}(\text{SR})_{18} > \text{Pt}_1\text{Au}_{24}(\text{SR})_{18}$. Interestingly, the $\text{Cu}_x\text{Au}_{25-x}(\text{SR})_{18}$ produced a homo-coupling product base on the Ullmann homo-coupling pathway, which was contrary to the other three cluster catalysts. However, DFT calculations showed that the adsorption energy of one PA molecule on the $\text{Pt}_1\text{Au}_{24}(\text{SR})_{18}$, $\text{Cu}_{1/2}\text{Au}_{24/23}(\text{SR})_{18}$, and $\text{Au}_{25}(\text{SR})_{18}$ nanoclusters was very similar (-0.50 to -0.52 eV, Table 6). The adsorption energy of one IB molecule onto the $\text{Pt}_1\text{Au}_{24}(\text{SR})_{18}$, $\text{Ag}_{1/2}\text{Au}_{24/23}(\text{SR})_{18}$, and $\text{Au}_{25}(\text{SR})_{18}$ was also very similar (-0.59 to -0.61 eV, Table 6). These results suggested that the adsorption process of the PA and IB onto the alloy clusters was not the key step during the coupling reactions. Generally, the catalytic activity was largely affected by the electronic

effect in the core of bimetallic clusters (i.e., $\text{Pt}_1\text{Au}_{12}$, $\text{Cu}_x\text{Au}_{13-x}$, $\text{Ag}_x\text{Au}_{13-x}$, and Au_{13}), and the selectivity of the product is primarily turned by the atomic type on the shell of $\text{M}_x\text{Au}_{12-x}$ [51,57].

4.4. A^3 -Coupling

A^3 -coupling reactions, where three reactants (aldehydes, amines, and alkynes) react each other in one-pot to yield only one product, have attracted overwhelming interest in the past decade. The A^3 -coupling is favorable from environmental and economic perspectives: more efficient and less waste [58–61]. The A^3 -coupling reactions involve new C–C and C–N bond formation in one procedure. The alkyne activation was deemed as the key step for the A^3 -coupling; the aldehydes could react with amines spontaneously. Hence, the gold clusters should be active in this reaction, because the cluster catalyst has exhibited the capacity of the alkyne activation in the semi-hydrogenation of terminal alkynes [36].

The catalytic performance of the $\text{Au}_{25}(\text{PPh}_3)_{10}(\text{PA})_5\text{X}_2$ was investigated in different solvents and reaction temperatures [62]. The most prominent feature was that the polarity of the solvent had a great influence on catalytic activity. The TiO_2 -supported Au_{25} catalyst gave higher activity in the polar solvents. The gold clusters also showed good recyclability. Interestingly, the cluster catalyst showed no conversion using ketones as reactants (Figure 8), which was completely different from the catalytic behaviors of the gold complexes and bare gold nanoparticles. Therefore, the electronic factors and steric hindrance of the substituents had significant effects on the reaction conversion rate.

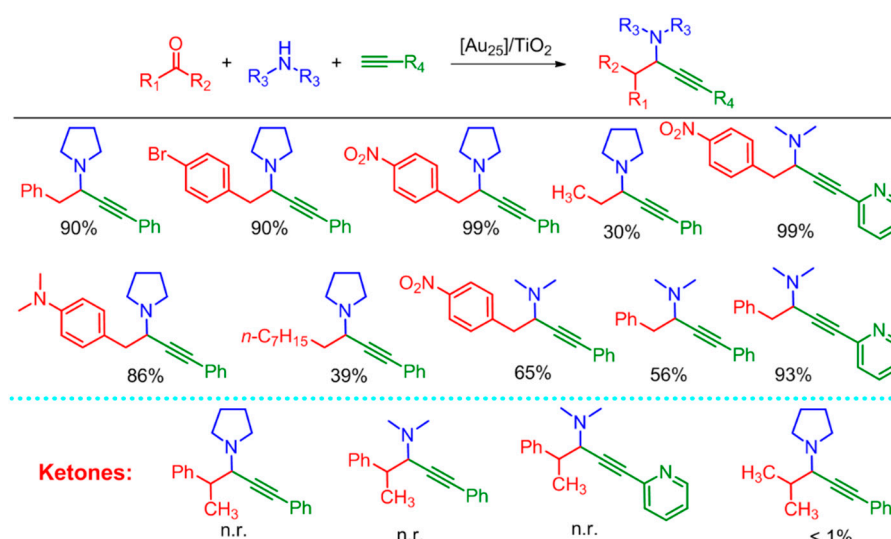


Figure 8. Catalytic results over the $\text{Au}_{25}(\text{PPh}_3)_{10}(\text{PA})_5\text{X}_2$ ($[\text{Au}_{25}]/\text{TiO}_2$) catalysts in the A^3 -coupling reaction. Reaction conditions: 100 mg catalyst (1 wt.% cluster loading), 1.0 mmol benzaldehyde, 1.2 mmol piperidine, 1.3 mmol phenylacetylene, 5 mL water, 100 °C, 18 h, under a N_2 atmosphere.

An induction period (0 to 3 h) appeared and the conversion slightly increased during the induction period. After the induction period, the reaction conversion of gold clusters significantly increased in the time evolution for A^3 -coupling [62]. The results showed that some phosphine ligands are removed to generate catalytic active sites, which associates with the surface gold atoms. Further research found that the capped phosphine ligands can be selectively removed in the case of $\text{Au}_{11}(\text{PPh}_3)_7\text{X}_3$ with the aid of base (e.g., pyridine), evidenced by UV-vis and ESI-MS analyses [63].

Finally, the catalytic mechanism over the gold clusters was studied by DFT calculations. Firstly, the phosphine ligand is detached in the presence of the reaction system, and then the uncovered Au atoms are exposed to the reactants. Next, the PA molecules are adsorbed onto the M1 site via the interaction of $\text{Au}\cdots$ whole triple bond, Figure 9. Further, a terminal hydrogen deprotonation occurs in

the presence of amine (e.g., $\text{HN}(\text{CH}_3)_2$). The iminium ion ($\text{H}_2\text{C}=\text{N}(\text{CH}_3)_2^+$) interacts with the $\text{PhC}\equiv\text{C}$ -on site M1 and finally give rise to the final product (i.e., propargylamine) [62].

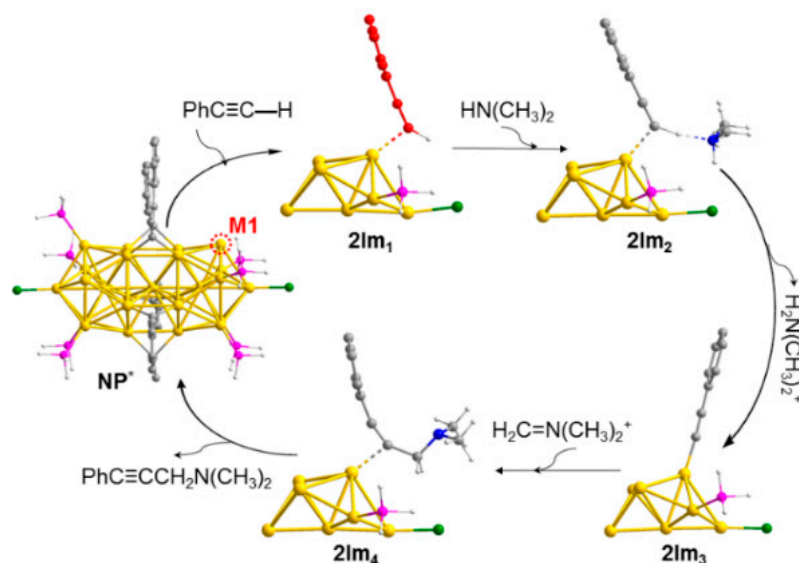


Figure 9. Proposed mechanism for the $[\text{Au}_{25}(\text{PH}_3)_{10}(\text{PA})_5\text{Cl}_2]^{2+}$ -catalyzed A^3 -coupling reaction. Reproduced with permission from [62]. Elsevier, 2016.

Further, Jin et al. reported Au_{38} nanocluster-catalyzed the A^3 -coupling reaction [64]. They argued that the synergistic effect of the partial positive charged Au surface ($\text{Au}^{\delta+}$, $0 < \delta < 1$) and the electron-rich Au_{23} kernel were responsible for the catalytic behaviors. Li et al. found that cadmium doped Au_{13} nanocluster also showed catalytic activity in the A^3 -coupling [65]. The cooperation between the exerted cadmium atoms and the neighbor gold atoms on the surface of Au_{13} icosahedron are tentatively deemed as the active sites in the cross-coupling reactions.

5. Summary and Outlook

In the past decade years, remarkable advances have been made in developing catalytic applications of gold nanoclusters, which is a new perspective for gold nanocatalysis, especially in carbon–carbon cross-coupling reactions. These gold nanoclusters were more efficient in the cross C–C coupling reactions in this Review. The higher catalytic activity was mainly because of the distinctive frame structure and electronic properties of the gold nanoclusters and the protecting ligands. However, some of the gold nanoclusters with the protection of thiolate/phosphine could not stay intact under the harsh reaction conditions during the catalysis processes, leading to a decrease or even disappearance of catalytic activity due to the increasing size of formed particles. How to maintain the stability of gold nanoclusters during the catalysis has become a major challenge and subject for future research.

The present review demonstrated that CeO_2 and TiO_2 oxides have been observed to be excellent supports for gold nanoclusters [66]. Few studies have been done on other oxides. Developing new types of supports is another significant issue for substances such as zeolite [67,68], carbon materials (e.g., graphene or graphite oxide) [69,70], and MOFs [71]. For example, mesoporous materials, e.g., MOFs and zeolite, exhibited regular tunnels and cages and improved the stability of the Au clusters during the catalytic processes [72]. The tunnels and cages, by enriching concentration of the reactants, can also improve the catalytic activity. The steric effects of MOFs organic linker can improve the selectivity of products. In addition, the sites of Lewis acids and Bronstein acids in zeolites also can change the catalytic performance of the catalysts.

In a word, gold nanoclusters will be expected to be used into carbon–heteroatom cross-coupling reactions, which are not yet well investigated. The formed C–O and C–N bonds are very useful

drug intermediates [73]. Recently, some attempts have been reported in these categories, such as the cross-aldol condensation and Michael addition (forming C=C bonds) and photo-oxidation of amines to imines (C=N bonds) [10,74]. Future research on gold nanoclusters will contribute to fundamental researches and provide clues for the new design of efficient catalysts for other specific chemical processes.

Author Contributions: Investigation, Q.S. and Z.Q. (resources, Q.S. and Z.Q.; writing—original draft preparation, Q.S. and Z.Q.; writing—review and editing, H.X. and G.L.; supervision, G.L.; project administration, G.L.

Funding: This research was funded by National Natural Science Foundation of China (21665020), the Natural Science Foundation of Inner Mongolia Autonomous Region (2018BS02004), and the Program of Higher-level Talents of Inner Mongolia Agricultural University (NDYB2016-03) for financial support.

Conflicts of Interest: The authors declare no conflict of interest.

References

1. Haruta, M.; Yamada, N.; Kobayashi, T.; Iijima, S. Gold catalysts prepared by coprecipitation for low-temperature oxidation of hydrogen and of carbon-monoxide. *J. Catal.* **1989**, *115*, 301–309. [[CrossRef](#)]
2. Tsukuda, T.; Tsunoyama, H.; Sakurai, H. Aerobic oxidations catalyzed by colloidal nanogold. *Chem. Asian J.* **2011**, *6*, 736–748. [[CrossRef](#)]
3. Della, P.C.; Falletta, E.; Rossi, M. Update on selective oxidation using gold. *Chem. Soc. Rev.* **2012**, *41*, 350–369.
4. Li, G.; Qian, H.F.; Jin, R.C. Gold nanocluster-catalyzed selective oxidation of sulfide to sulfoxide. *Nanoscale* **2012**, *4*, 6714–6717. [[CrossRef](#)]
5. Liu, C.; Yan, C.Y.; Lin, J.Z.; Yu, C.L.; Huang, J.H.; Li, G. One-pot synthesis of Au₁₄₄(SCH₂Ph)₆₀ nanoclusters and their catalytic application. *J. Mater. Chem. A* **2015**, *3*, 20167–20173. [[CrossRef](#)]
6. Hashmi, A.S.K.; Hutchings, G.J. Gold catalysis. *Angew. Chem. Int. Ed.* **2006**, *45*, 7896–7936. [[CrossRef](#)]
7. Li, G.; Zeng, C.J.; Jin, R.C. Thermally robust Au₉₉(SPh)₄₂ nanoclusters for chemoselective hydrogenation of nitrobenzaldehyde derivatives in water. *J. Am. Chem. Soc.* **2014**, *136*, 3673–3679. [[CrossRef](#)]
8. Li, G.; Jiang, D.E.; Kumar, S.; Chen, Y.X.; Jin, R.C. Size dependence of atomically precise gold nanoclusters in chemoselective hydrogenation and active site structure. *ACS Catal.* **2014**, *4*, 2463–2469. [[CrossRef](#)]
9. Naya, S.; Kimura, K.; Tada, H. One-step selective aerobic oxidation of amines to imines by gold nanoparticle-loaded Rutile titanium(IV) oxide plasmon photocatalyst. *ACS Catal.* **2013**, *3*, 10–13. [[CrossRef](#)]
10. Chen, H.J.; Liu, C.; Wang, M.; Zhang, C.F.; Luo, N.C.; Wang, Y.H.; Abroshan, H.; Li, G.; Wang, F. Visible light gold nanocluster photocatalyst: Selective aerobic oxidation of amines to imines. *ACS Catal.* **2017**, *7*, 3632–3638. [[CrossRef](#)]
11. Taketoshi, A.; Haruta, M. Size- and structure-specificity in catalysis by gold clusters. *Chem. Lett.* **2014**, *43*, 380–387. [[CrossRef](#)]
12. Lohse, S.E.; Murphy, C.J. The quest for shape control: A history of gold nanorod synthesis. *Chem. Mater.* **2013**, *25*, 1250–1261. [[CrossRef](#)]
13. Lu, C.L.; Prasad, K.S.; Wu, H.L.; Ho, J.A.A.; Huang, M.H. Au nanocube-directed fabrication of Au-Pd core-shell nanocrystals with tetrahedral, concave octahedral, and octahedral structures and their electrocatalytic activity. *J. Am. Chem. Soc.* **2010**, *132*, 14546–14553. [[CrossRef](#)]
14. Zhang, J.; Li, Z.; Zheng, K.; Li, G. Synthesis and characterization of size-controlled atomically-precise gold clusters. *Phys. Sci. Rev.* **2018**, *3*. [[CrossRef](#)]
15. Jin, R.C. Atomically precise metal nanoclusters: Stable sizes and optical properties. *Nanoscale* **2015**, *7*, 1549–1565. [[CrossRef](#)]
16. Li, G.; Jin, R.C. Atomically precise gold nanoclusters as new model catalysts. *Acc. Chem. Res.* **2013**, *46*, 1749–1758. [[CrossRef](#)]
17. Yamazoe, S.; Koyasu, K.; Tsukuda, T. Nonscalable oxidation catalysis of gold clusters. *Acc. Chem. Res.* **2014**, *47*, 816–824. [[CrossRef](#)] [[PubMed](#)]
18. Li, Z.M.; Abroshan, H.; Liu, C.; Li, G. A Critical review on the catalytic applications of non-metallic gold nanoclusters: Selective oxidation, hydrogenation, and coupling reactions. *Curr. Org. Chem.* **2017**, *21*, 476–488. [[CrossRef](#)]
19. Li, G.; Jin, R.C. Catalysis by gold NPs: Carbon-carbon coupling reactions. *Nanotechnol. Rev.* **2013**, *5*, 529–545.

20. Zhou, Y.; Li, G. A Critical review on carbon-carbon coupling over ultra-small gold nanoclusters. *Acta Phys.-Chim. Sin.* **2017**, *33*, 1297–1309.
21. Alonso, F.; Beletskaya, I.P.; Yus, M. Non-conventional methodologies for transition-metal catalysed carbon-carbon coupling: A critical overview. Part 2: The Suzuki reaction. *Tetrahedron* **2008**, *64*, 3047–3101. [[CrossRef](#)]
22. Seechurn, C.; Kitching, M.O.; Colacot, T.J.; Snieckus, V. Palladium-catalyzed cross-coupling: A historical contextual perspective to the 2010 Nobel Prize. *Angew. Chem. Int. Ed.* **2012**, *51*, 5062–5085. [[CrossRef](#)] [[PubMed](#)]
23. Fihri, A.; Bouhrara, M.; Nekoueishahraki, B.; Polshettiwar, V. Nanocatalysts for Suzuki cross-coupling reactions. *Chem. Soc. Rev.* **2011**, *40*, 5181–5203. [[CrossRef](#)]
24. Kanuru, V.K.; Kyriakou, G.; Beaumont, S.K.; Papageorgiou, A.C.; Watson, D.J.; Lambert, R.M. Sonogashira coupling on an extended gold surface in vacuo: Reaction of phenylacetylene with iodobenzene on Au(111). *J. Am. Chem. Soc.* **2010**, *132*, 8081–8086. [[CrossRef](#)]
25. González-Arellano, C.; Abad, A.; Corma, A.; García, H.; Iglesias, M.; Sánchez, F. Catalysis by gold(I) and gold(III): A parallelism between homo- and heterogeneous catalysts for copper-free Sonogashira cross-coupling reactions. *Angew. Chem. Int. Ed.* **2007**, *46*, 1536–1538. [[CrossRef](#)] [[PubMed](#)]
26. Lin, J.Z.; Abroshan, H.; Liu, C.; Zhu, M.Z.; Li, G.; Haruta, M. Sonogashira cross-coupling on the Au(111) and Au(100) facets of gold nanorod catalysts: Experimental and computational investigation. *J. Catal.* **2015**, *330*, 354–361. [[CrossRef](#)]
27. Li, G.; Zeng, C.J.; Jin, R.C. Chemoselective hydrogenation of nitrobenzaldehyde to nitrobenzyl alcohol with unsupported Au nanorod catalysts in water. *J. Phys. Chem. C* **2015**, *119*, 11143–11147. [[CrossRef](#)]
28. Murphy, C.J.; Gole, A.M.; Hunyadi, S.E.; Stone, J.W.; Sisco, P.N.; Alkilany, A.; Kinard, B.E.; Hankins, P. Chemical sensing and imaging with metallic nanorods. *Chem. Commun.* **2008**, *5*, 544–547. [[CrossRef](#)]
29. Bai, X.T.; Gao, Y.N.; Liu, H.G.; Zheng, L.Q. Synthesis of amphiphilic ionic liquids terminated gold nanorods and their superior catalytic activity for the reduction of nitro compounds. *J. Phys. Chem. C* **2009**, *113*, 17730–17736. [[CrossRef](#)]
30. Boronat, M.; Combata, D.; Concepción, P.; Corma, A.; García, H.; Juárez, R.; Laursen, S.; López-Castro, J.D. Making C-C bonds with gold: Identification of selective gold sites for homo- and cross-coupling reactions between iodobenzene and alkynes. *J. Phys. Chem. C* **2012**, *116*, 24855–24867. [[CrossRef](#)]
31. Boronat, M.; Corma, A. Molecular approaches to catalysis naked gold NPs as quasi-molecular catalysts for green processes. *J. Catal.* **2011**, *284*, 138–147. [[CrossRef](#)]
32. Corma, A.; Juárez, R.; Boronat, M.; Sánchez, F.; Iglesias, M.; García, H. Gold catalyzes the Sonogashira coupling reaction without the requirement of palladium impurities. *Chem. Commun.* **2011**, *47*, 1446–1448. [[CrossRef](#)] [[PubMed](#)]
33. Zhang, J.; Zhou, Y.; Zheng, K.; Abroshan, H.; Kauffman, D.R.; Sun, J.; Li, G. Diphosphine-induced chiral propeller arrangement of gold nanoclusters for singlet oxygen photogeneration. *Nano Res.* **2018**, *11*, 5787–5798. [[CrossRef](#)]
34. Zhu, M.; Aikens, C.M.; Hollander, F.J.; Schatz, G.C.; Jin, R.C. Correlating the crystal structure of a thiol-protected Au₂₅ cluster and optical properties. *J. Am. Chem. Soc.* **2008**, *130*, 5883–5885. [[CrossRef](#)]
35. Zheng, K.; Zhang, J.W.; Zhao, D.; Yang, Y.; Li, Z.M.; Li, G. Motif Mediated Au₂₅(SPh)₅(PPh₃)₁₀X₂ Nanorod of Conjugated Electron Delocalization. *Nano Res.* **2019**, *12*, 501–507. [[CrossRef](#)]
36. Li, G.; Jin, R.C. Gold nanocluster-catalyzed semihydrogenation: A unique activation pathway for terminal alkynes. *J. Am. Chem. Soc.* **2014**, *136*, 11347–11354. [[CrossRef](#)]
37. Li, Z.M.; Liu, C.; Abroshan, H.; Kauffman, D.R.; Li, G. Au₃₈S₂(SAdm)₂₀ Photocatalyst for One-Step Selective Aerobic Oxidations. *ACS Catal.* **2017**, *7*, 3368–3374. [[CrossRef](#)]
38. Yan, C.Y.; Liu, C.; Abroshan, H.; Li, Z.M.; Qiu, R.; Li, G. Surface modification of adamantane-terminated gold nanoclusters using cyclodextrins. *Phys. Chem. Chem. Phys.* **2016**, *18*, 23358–23364. [[CrossRef](#)] [[PubMed](#)]
39. Zhang, C.; Chen, Y.; Wang, H.; Li, Z.; Zheng, K.; Li, S.; Li, G. Transition-metal-mediated catalytic properties of CeO₂-supported gold clusters in aerobic alcohol oxidation. *Nano Res.* **2018**, *11*, 2139–2148. [[CrossRef](#)]
40. Kumar, S.S.; Kwak, K.; Lee, D. Amperometric sensing based on glutathione protected Au₂₅ nanoparticles and their pH dependent electrocatalytic activity. *Electroanalysis* **2011**, *23*, 2116–2124. [[CrossRef](#)]

41. Kauffman, D.R.; Alfonso, D.; Matranga, C.; Qian, H.; Jin, R. Experimental and computational investigation of Au₂₅ clusters and CO₂: A unique interaction and enhanced electrocatalytic activity. *J. Am. Chem. Soc.* **2012**, *134*, 10237–10243. [[CrossRef](#)] [[PubMed](#)]
42. Monnier, F.; Taillefer, M. Catalytic C-C, C-N, and C-O Ullmann-type coupling reactions. *Angew. Chem. Int. Ed.* **2009**, *48*, 6954–6971. [[CrossRef](#)] [[PubMed](#)]
43. Yu, C.L.; Li, G.; Kumar, K.S.; Kawasaki, H.; Jin, R.C. Stable Au₂₅(SR)₁₈/TiO₂ Composite nanostructure with enhanced visible light photocatalytic activity. *J. Phys. Chem. Lett.* **2013**, *4*, 2847–2852. [[CrossRef](#)]
44. Chen, H.J.; Liu, C.; Wang, M.; Zhang, C.F.; Li, G.; Wang, F. Thermally robust silica-enclosed Au₂₅ nanocluster and its catalysis. *Chin. J. Catal.* **2016**, *37*, 1787–1793. [[CrossRef](#)]
45. Li, G.; Liu, C.; Lei, Y.; Jin, R.C. Au₂₅ nanocluster-catalyzed Ullmann-type homocoupling reaction of aryl iodides. *Chem. Commun.* **2012**, *48*, 12005–12007. [[CrossRef](#)] [[PubMed](#)]
46. Li, G.; Abroshan, H.; Liu, C.; Zhuo, S.; Li, Z.M.; Xie, Y.; Kim, H.J.; Rosi, N.L.; Jin, R.C. Tailoring the electronic and catalytic properties of Au₂₅ nanoclusters via ligand engineering. *ACS Nano* **2016**, *10*, 7998–8005. [[CrossRef](#)] [[PubMed](#)]
47. Abroshan, H.; Li, G.; Lin, J.Z.; Kim, H.J.; Jin, R.C. Molecular mechanism for the activation of Au₂₅(SCH₂CH₂Ph)₁₈ nanoclusters by imidazolium-based ionic liquids for catalysis. *J. Catal.* **2016**, *337*, 72–79. [[CrossRef](#)]
48. Li, G.; Abroshan, H.; Chen, Y.X.; Jin, R.C.; Kim, H.J. Experimental and mechanistic understanding of aldehyde hydrogenation using Au₂₅ nanoclusters with Lewis acids: Unique sites for catalytic reactions. *J. Am. Chem. Soc.* **2015**, *137*, 14295–14304. [[CrossRef](#)]
49. Li, G.; Jiang, D.E.; Liu, C.; Yu, C.L.; Jin, R.C. Oxide-supported atomically precise gold nanocluster for catalyzing Sonogashira cross-coupling. *J. Catal.* **2013**, *306*, 177–183. [[CrossRef](#)]
50. Kumara, C.; Aikens, C.M.; Dass, A. X-ray crystal structure and theoretical analysis of Au_{25–x}Ag_x(SCH₂CH₂Ph)₁₈-alloy. *J. Phys. Chem. Lett.* **2014**, *5*, 461–466. [[CrossRef](#)]
51. Li, W.L.; Liu, C.; Abroshan, H.; Ge, Q.J.; Yang, X.J.; Xu, H.Y.; Li, G. Catalytic CO oxidation using bimetallic M_xAu_{25–x} clusters: A combined experimental and computational study on doping effects. *J. Phys. Chem. C* **2016**, *120*, 10261–10267. [[CrossRef](#)]
52. Jiang, D.E.; Whetten, R.L. Magnetic doping of a thiolated-gold superatom: First-principles density functional theory calculations. *Phys. Rev. B* **2009**, *80*, 115402. [[CrossRef](#)]
53. Qian, H.F.; Jiang, D.E.; Li, G.; Gayathri, C.; Das, A.; Gil, R.R.; Jin, R.C. Monoplatinum Doping of Gold Nanoclusters and Catalytic Application. *J. Am. Chem. Soc.* **2012**, *134*, 16159–16162. [[CrossRef](#)]
54. Xie, S.H.; Tsunoyama, H.; Kurashige, W.; Negishi, Y.; Tsukuda, T. Enhancement in aerobic alcohol oxidation catalysis of Au₂₅ clusters by single Pd atom doping. *ACS Catal.* **2012**, *2*, 1519–1523. [[CrossRef](#)]
55. Li, G.; Jin, R.C. Atomic level tuning of the catalytic properties: Doping effects of 25-atom bimetallic nanoclusters on styrene oxidation. *Catal. Today* **2016**, *278*, 187–191. [[CrossRef](#)]
56. Li, Z.M.; Yang, X.J.; Liu, C.; Wang, J.; Li, G. Effects of doping in 25-atom bimetallic nanocluster catalysts for carbon-carbon coupling reaction of iodoanisole and phenylacetylene. *Proc. Nat. Sci. Mater. Int.* **2016**, *26*, 477–482. [[CrossRef](#)]
57. Qin, Z.; Zhao, D.; Zhao, L.; Xiao, Q.; Wu, T.; Zhang, J.; Wan, C.-Q.; Li, G. Tailoring the Stability, Photocatalysis and Photoluminescence Properties of Au₁₁ Nanocluster via Doping Engineering. *Nanoscale Adv.* **2019**, *2*. [[CrossRef](#)]
58. Dömling, A. Recent developments in isocyanide based multicomponent reactions in applied chemistry. *Chem. Rev.* **2006**, *106*, 17–89. [[CrossRef](#)]
59. Ganem, B. Strategies for innovation in multicomponent reaction design. *Acc. Chem. Res.* **2009**, *42*, 463–472. [[CrossRef](#)]
60. Climent, M.J.; Corma, A.; Iborra, S. Homogeneous and heterogeneous catalysts for multicomponent reactions. *RSC Adv.* **2012**, *2*, 16–58. [[CrossRef](#)]
61. Wei, C.M.; Li, C.J. A highly efficient three-component coupling of aldehyde, alkyne, and amines via C-H activation catalyzed by gold in water. *J. Am. Chem. Soc.* **2003**, *125*, 9584–9585. [[CrossRef](#)] [[PubMed](#)]
62. Chen, Y.D.; Liu, C.; Abroshan, H.; Li, Z.M.; Wang, J.; Li, G.; Haruta, M. Phosphine/phenylacetylide-ligated Au clusters for multicomponent coupling reactions. *J. Catal.* **2016**, *337*, 287–294. [[CrossRef](#)]
63. Liu, C.; Abroshan, H.; Yan, C.Y.; Li, G.; Haruta, M. One-pot synthesis of Au₁₁(PPh₂Py)₇Br₃ for the highly chemoselective hydrogenation of nitrobenzaldehyde. *ACS Catal.* **2016**, *6*, 92–99. [[CrossRef](#)]

64. Li, Q.; Das, A.; Wang, S.X.; Chen, Y.X.; Jin, R.C. Highly efficient three-component coupling reaction catalysed by atomically precise ligand-protected Au₃₈(SC₂H₄Ph)₂₄ nanoclusters. *Chem. Commun.* **2016**, *52*, 14298–14301. [[CrossRef](#)]
65. Li, M.; Tian, S.; Wu, Z. Improving the catalytic activity of Au₂₅ nanocluster by peeling and doping. *Chin. J. Chem.* **2017**, *35*, 567–571. [[CrossRef](#)]
66. Wen, Z.Y.; Li, Z.M.; Ge, Q.J.; Zhou, Y.; Sun, J.; Li, G. Robust nickel cluster@Mes-HZSM-5 composite nanostructure with enhanced catalytic activity in the DTG reaction. *J. Catal.* **2018**, *363*, 26–33. [[CrossRef](#)]
67. Li, Z.M.; Li, W.L.; Abroshan, H.; Ge, Q.J.; Zhou, Y.; Zhang, C.L.; Li, G.; Jin, R.C. Dual Effects of Water Vapor over Ceria-Supported Gold Clusters. *Nanoscale* **2018**, *10*, 6558–6565. [[CrossRef](#)]
68. Wang, F.; Wen, Z.; Fang, Q.; Ge, Q.; Sun, J.; Li, G. Manganese cluster induce the control synthesis of RHO- and CHA-type silicoaluminophosphates for dimethylether to light olefin conversion. *Fuel* **2019**, *244*, 104–109. [[CrossRef](#)]
69. Guo, S.; Zhang, S.H.; Fang, Q.H.; Abroshan, H.; Kim, H.; Haruta, M.; Li, G. Gold-palladium nanoalloys supported by graphene oxide and lamellar TiO₂ for direct synthesis of hydrogen peroxide. *ACS Appl. Mater. Interfaces* **2018**, *10*, 40599–40607. [[CrossRef](#)]
70. Liu, C.; Zhang, J.Y.; Huang, J.H.; Zhang, C.L.; Hong, F.; Zhou, Y.; Li, G.; Haruta, M. Efficient aerobic oxidation of glucose to gluconic acid over activated carbon-supported gold clusters. *ChemSusChem* **2017**, *10*, 1976–1980. [[CrossRef](#)]
71. Vilhelmsen, L.B.; Walton, K.S.; Sholl, D.S. Structure and mobility of metal clusters in MOFs: Au, Pd, and AuPd clusters in MOF-74. *J. Am. Chem. Soc.* **2012**, *134*, 12807–12816. [[CrossRef](#)] [[PubMed](#)]
72. Chen, H.; Li, Z.; Qin, Z.; Kim, H.J.; Abroshan, H.; Li, G. Silica-encapsulated gold nanoclusters for efficient acetylene hydrogenation to ethylene. *ACS Appl. Nano Mater.* **2019**. [[CrossRef](#)]
73. Ciobanu, M.; Cojocaru, B.; Teodorescu, C.; Vasiliu, F.; Coman, S.M.; Leitner, W.; Parvulescu, V.I. Heterogeneous amination of bromobenzene over titania-supported gold catalysts. *J. Catal.* **2012**, *296*, 43–54. [[CrossRef](#)]
74. Fang, Q.; Qin, Z.; Shi, Y.; Liu, F.; Barkaoui, S.; Abroshan, H.; Li, G. Au/NiO composite: A catalyst for one-pot cascade conversion of furfural. *ACS Appl. Energy Mater.* **2019**, *2*, 2654–2661. [[CrossRef](#)]



© 2019 by the authors. Licensee MDPI, Basel, Switzerland. This article is an open access article distributed under the terms and conditions of the Creative Commons Attribution (CC BY) license (<http://creativecommons.org/licenses/by/4.0/>).